Spectral Measurements of Geosynchronous Satellites During Glint Season

Ryan M. Tucker, Evan M. Weld, Francis K. Chun, and Roger D. Tippets
Department of Physics, U.S. Air Force Academy

ABSTRACT

Operational communication geosynchronous satellites are typically large structures with long solar panels that maintain a stable attitude relative to the earth and sun. During the equinox periods of the year, the geometry of the satellite, sun and an earth observer is favorable for a condition to occur called a glint, or specular reflection. It is presumed that the glint is caused by the satellite solar panels and has been observed in the past using broadband photometry techniques. In this paper, we present the first observations of a glint from two satellites, Wildblue-1 and DirecTV-12, as measured across the visible spectrum using slitless spectroscopy techniques. It is clear from the results that the wavelength where the glint maximum occurs can sometimes move toward the blue end of the spectrum relative to the time periods before and after the glint. This is consistent with the presumption that the solar panels are the main cause of the satellite glint. It is also clear from the spectral data that there is small-scale spatial and temporal structure associated with a glint that may not be seen in broadband photometry. We believe that these small-scale features can be exploited to discern satellite features such as solar panel orientation and secondary mechanical structures.

1. INTRODUCTION

Man-made satellites serve a plethora of purposes from navigation to remote sensing. Geostationary orbits are among the most important types of orbits in that satellites can orbit the earth at a rate which matches the speed of the rotation of the earth, in effect causing these satellites to appear fixed above the same point on earth. These geostationary satellites (GEOs) facilitate communications, weather forecasting, and intelligence operations. Military and civilian organizations across the world utilize the approximate 400 operational GEOs for everyday activities and could not operate at normal capacity without them.

Within the space community the light reflected off of satellites has been observed in a variety of means, from broadband photometry to spectroscopy [1-5]. The light, which primarily originates from the sun, reflects off the solar panels and busses of satellites and can easily be observed by an optical telescope. Observations are collected and the reflected light is separated into a broad spectrum of wavelengths. This general technique is referred to as spectroscopy. Across the spectrum certain wavelengths have greater intensities than others, but to first order looks very much like the solar spectrum. Researchers can take this data and discern a number of satellite features such as the composition of the satellite based on the relative intensities in different sections of the spectra or satellite solar panel orientation.

Spectral measurements using a diffraction grating are not new to the community [4, 5]. *Hoag and Schroeder* developed rudimentary slitless spectroscopic techniques in 1970 [6]. Fig. 1 is a sampling of photographs of collected spectra with various exposure times ranging from 30 seconds to 50 minutes. The top of the photographs are oriented north and the left sides are oriented east. The photographs' field of view covers around 30 minutes-of-arc, but the images in Fig. 1 are small sections of those original photographs. The small dots to the left of the black smear are the zero-order spectra. The "zeroth-order" spectrum is in line with the source, and is used as the center point for spectral measurements. The distance from the center of the zero-order spectrum represents a wavelength according to a dispersion relationship. Hoag's dispersion was 1,260 Å/mm; for example, a measurement at 3 mm away from the zero-order spectrum corresponds to a photon of wavelength 3,780 Å. They did not have the computational tools to parse out the spectra to more detail than identifying Balmer and Lyman series absorption lines, and they could not measure individual photon counts.

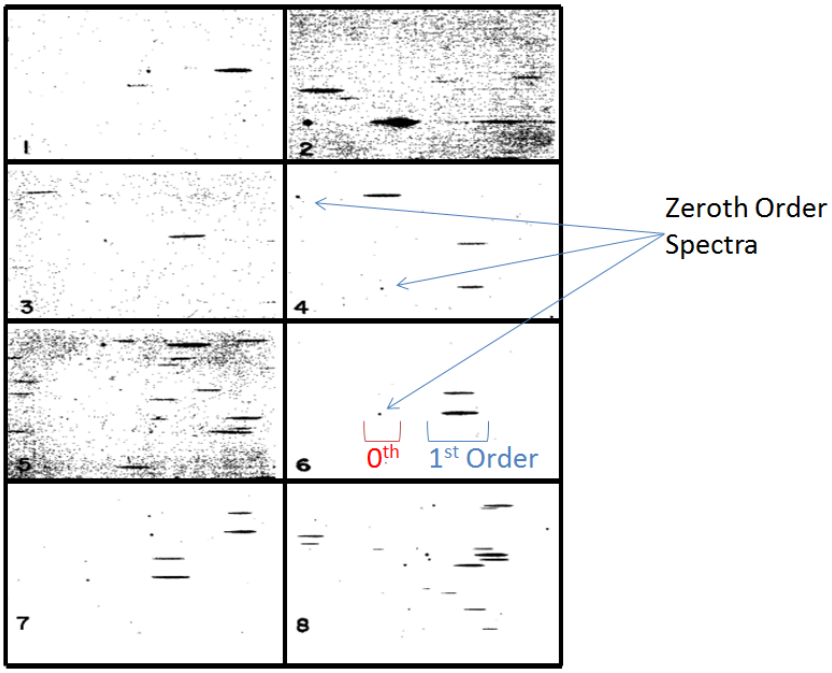

Fig. 1. Example of slitless spectroscopy images from Hoag and Schroeder [6].

The goal of this research is to measure the optical signature of a GEO satellite under a certain illumination condition favorable to glints. Previously, observations of glints using multi-color, broadband photometry show a characteristic peak in intensity around the zero phase angle [7], however to the best of our knowledge, there has not been any observations of glints made spectrally. To do so, we exploit slitless spectroscopy techniques developed and calibrated by U.S. Air Force Academy physics cadets in previous senior capstone research projects [8]. In this paper, we will discuss satellite glints and its cause, present our current methodology, show observational results for two GEO satellites, and end with conclusions and future work.

2. SATELLITE GLINTS

Geostationary satellites are used for communication and navigation, among other purposes as mentioned above. By observing and characterizing the satellites through spectroscopy, we can catalog and discriminate between the satellites. The measurements we make can be used to attempt to find patterns and irregularities with the satellite, which can enhance our space situational awareness (SSA) of the space environment by alerting us to changes to normal behavior or appearance. Lastly, because satellites and debris fill the limited space in which operational geostationary satellites orbit, we track objects in space to avoid collisions and prevent the creation of more debris.

Glints are a unique opportunity to observe optical signatures that can perhaps give insight into the composition, size and orientation of the solar panels on each of the geosynchronous satellites [9]. A glint is a specular (mirror-like) reflection due to a unique geometry when the inclination of a GEO satellite's orbit approaches that of the ecliptic plane (usually around the two equinox periods). For this research, we observed the glints that occurred around the vernal equinox for two GEO satellites, Wildblue-1 and DirecTV-12. Fig. 2 shows an artist rendition of the satellites. Both Wildblue-1 (Space Systems/Loral 1300 spacecraft bus) and DirecTV-12 (Boeing 702 spacecraft bus) are U.S. communications satellites with large deployable solar panels. Thus it will be of interest to see how there spectra compare. Most communications satellite owner/operators fly their satellite so that the solar panels are oriented in a north-south direction.

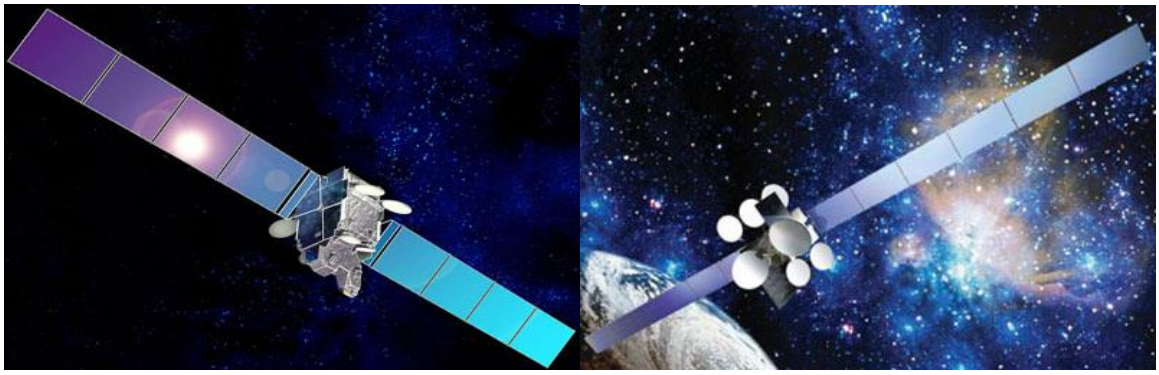

Fig. 2. Artist rendition of Wildblue-1 (left) and DirecTV-12 (right). Images taken from Gunter's Space Page (http://space.skyrocket.de/).

Glints occur when the bisector of the angle between the sunlight vector and the observer vector (i.e., the phase-angle bisector) is parallel to the normal vector of the solar panels on the satellite. This can be seen in Fig. 3 below which shows the geometrical condition for glinting. Normally, when the phase angle is not optimal for glinting, the sunlight reflected off the satellite is predominantly diffusive, dispersing in all directions, and the reflected light that reaches the ground observer may not display distinct spectral features of the material off which it was reflected. During glints, however, the reflected light can perhaps include spectral characteristics of the material off of which it reflects. For instance, satellite solar panels are designed to absorb much of the visual spectrum, especially the red part which contains most of the solar energy flux, thus we surmise that during a glint, more light would be reflected from the blue end of the solar spectrum. Additionally, if a satellite glint is primarily due to specular reflection off of the solar panels, the occurrence of a glint relative to solar phase angle or even the number of glints can provide insight as to how a satellite owner orients their solar panels relative to each other and to the sun.

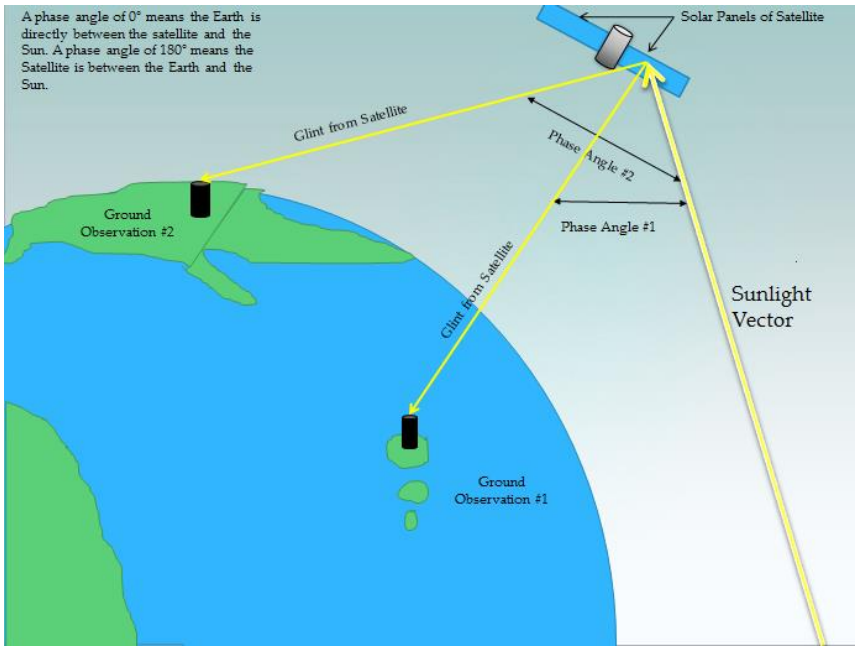

Fig. 3. Geometrical representation of a glint.

3. METHODS

The data processing algorithm we used is outlined in Fig. 4 below. The raw data collected from the telescope CCD goes through several refinement and reducation steps before we can start to analyze the results. This section will go into detail on the data processing techniques we used.

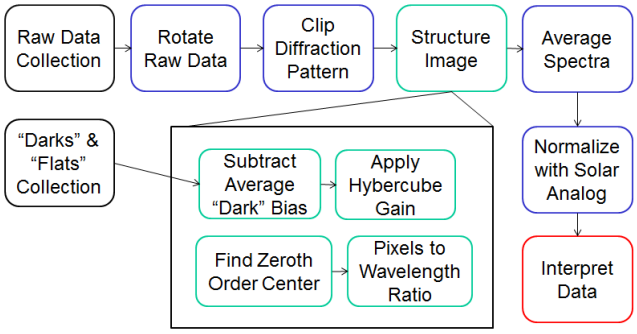

Fig. 4. Process and methodology used for this research project.

We collected data using the DFM Engineering f/8.2, 16-inch fast-tracking telescope at the USAFA Observatory. We collected images with an Apogee U47 CCD camera and saved them as 1,024 pixel by 1,024 pixel images. Thus the field of view in each of the saved images is 0.23 degrees or approximately 13 arc minutes on a side. We captured images of solar analogs and geostationary satellites through a 100 lines per millimeter diffraction grating. The theoretical resolution of the diffraction grating is $100 < R < 150$ depending on the wavelength, resulting in an average resolution of 26 angstroms [10].

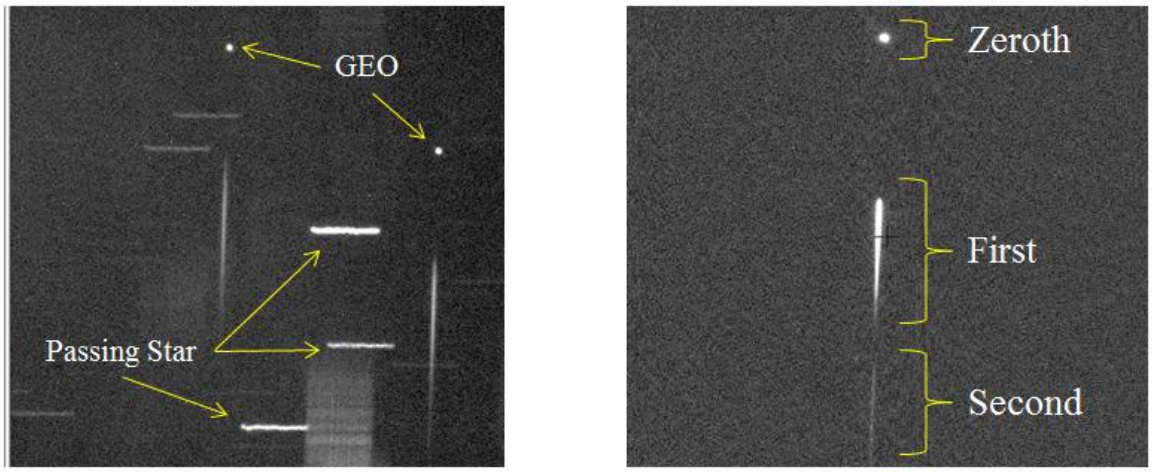

Fig. 5. Example raw images of spectra taken with the USAFA 16-inch telescope. The left panel shows two GEO satellites while the right panel is the star Alhena.

Two images from the CCD are shown above in Fig. 5. The picture to the right is the picture of the star Alhena through a 100 lines/mm grating. The zeroth order spectrum is seen at the top of the picture, with the first and higher order dispersion spectra below. The picture to the left shows two GEOs and several stars passing through the field of view. We adjusted the exposure time for each picture to prevent saturation of the image while achieving a reasonable signal to noise ratio. As you can see in Fig. 5 stars passing through the field of view will inevitably corrupt the satellite's dispersion patter in a few images. When this occurs, we remove the image from our processing to ensure our results are as pristine as possible. We further process the images using a computer reduction software program developed in MatLAB. Due to a small misalignment error of the diffraction grating relative to the camera's focal plane, the dispersion pattern on each CCD image is not aligned vertically in the image. Thus, we rotate the image so that the pattern is vertical (see Fig. 6). We then find the center of the zeroth order spectrum, and move down a narrow column ranging from 15 to 20 pixels wide to create an array of the intensity at each pixel from the top of the image to the bottom.

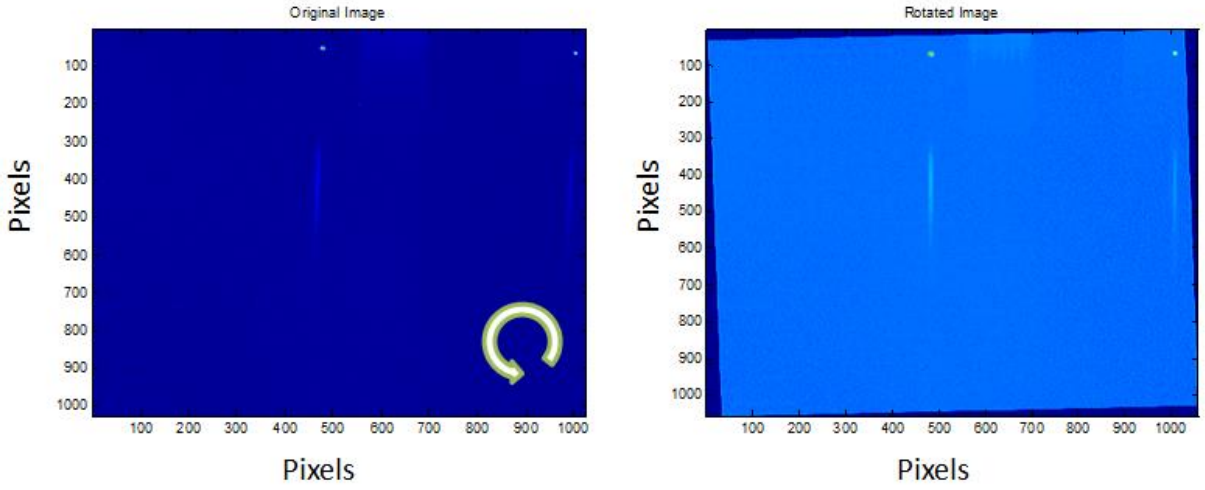

Fig. 6. Rotation of the image due to misalignment of the diffraction grating to camera's focal plane.

The arrays of clipped intensities are in units of pixels versus counts, so in order to investigate the wavelength dependencies of the spectra, we must convert the spectra from pixel space to wavelength space. To do so, we can use emission lines of Wolf-Rayet stars or absorption lines of calibration stars to determine the pixel-to-wavelength conversion for this telescope-camera system. We took spectra of the Wolf-Rayet star HD192163 to create our calibration that we applied to satellite spectra by matching pixel number to the known wavelength of emission lines. Fig. 7 below shows the emission spectrum for HD192163, which results in a pixel-to-wavelength conversion of:

$$\lambda=1.646*P+5.752 \qquad \text{(Eq. 1)}$$

Where λ is the calibrated wavelength and P is the distance from the zeroth order in pixels. The result of applying this conversion can be seen in Fig. 8.

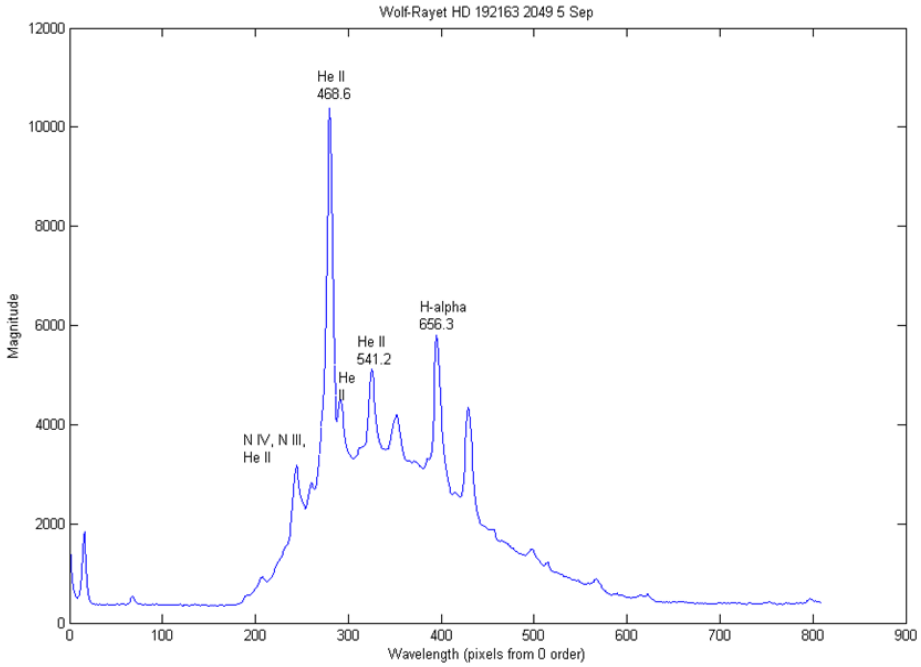

Fig. 7. Wolf-Rayet star spectra which shows emission lines at specific wavelengths [8].

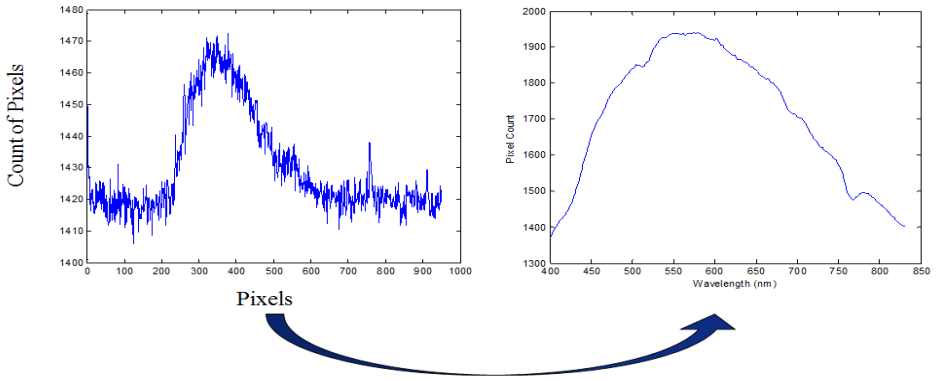

Fig. 8. Conversion of spectra from pixel space to wavelength space. The left panel is a single spectra while the right panel shows a spectra averaged from ~10 individual spectra.

We averaged several of these counts per second versus wavelength curves to find prevalent patterns in the wave shape. Some of the data are corrupted by passing stars, so to find which images are corrupted, we lined up several of the raw spectral curves and found irregularities. Fig. 9 below shows several of these curves. We removed the curves with sharp spikes, which represent passing stars, before averaging the curves.

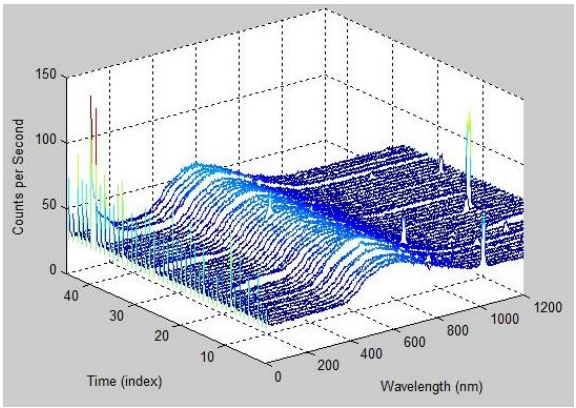

Fig. 9. Series of raw satellite spectra showing incidents of stars corrupting the spectra.

Ultimately, to be able to determine spectral features unique to satellite materials, we need to remove as much of the solar spectrum as possible. However since it is impossible to measure the solar spectrum during the same night as we measure satellite spectra, we have to use solar proxies such as solar analog stars. By definition, solar analog stars are photometrically similar to the Sun, with a temperature within 500 K from that of the Sun (roughly 5200 to 6300 K) [11]. We took spectra of a solar analog, HD84117, over the course of a night as a baseline for comparison. In Fig. 10 above you can see as expected, the intensity and profile of the spectra does not change over time. When we normalized the first order spectrum of each image to the zeroth order spectrum of that same image, the resulting spectrum looks relatively constant just like the initial intensity which was in counts per second. However, this normalized spectrum's intensity is now unit less and represents a relative fraction of the total light emitted by HD84117 as a function of wavelength. Further, Fig. 10 denotes the similar features that the intensity has with counts per seconds versus a normalized intensity. This is to be expected since this solar analog star is for the most part fairly constant in intensity.

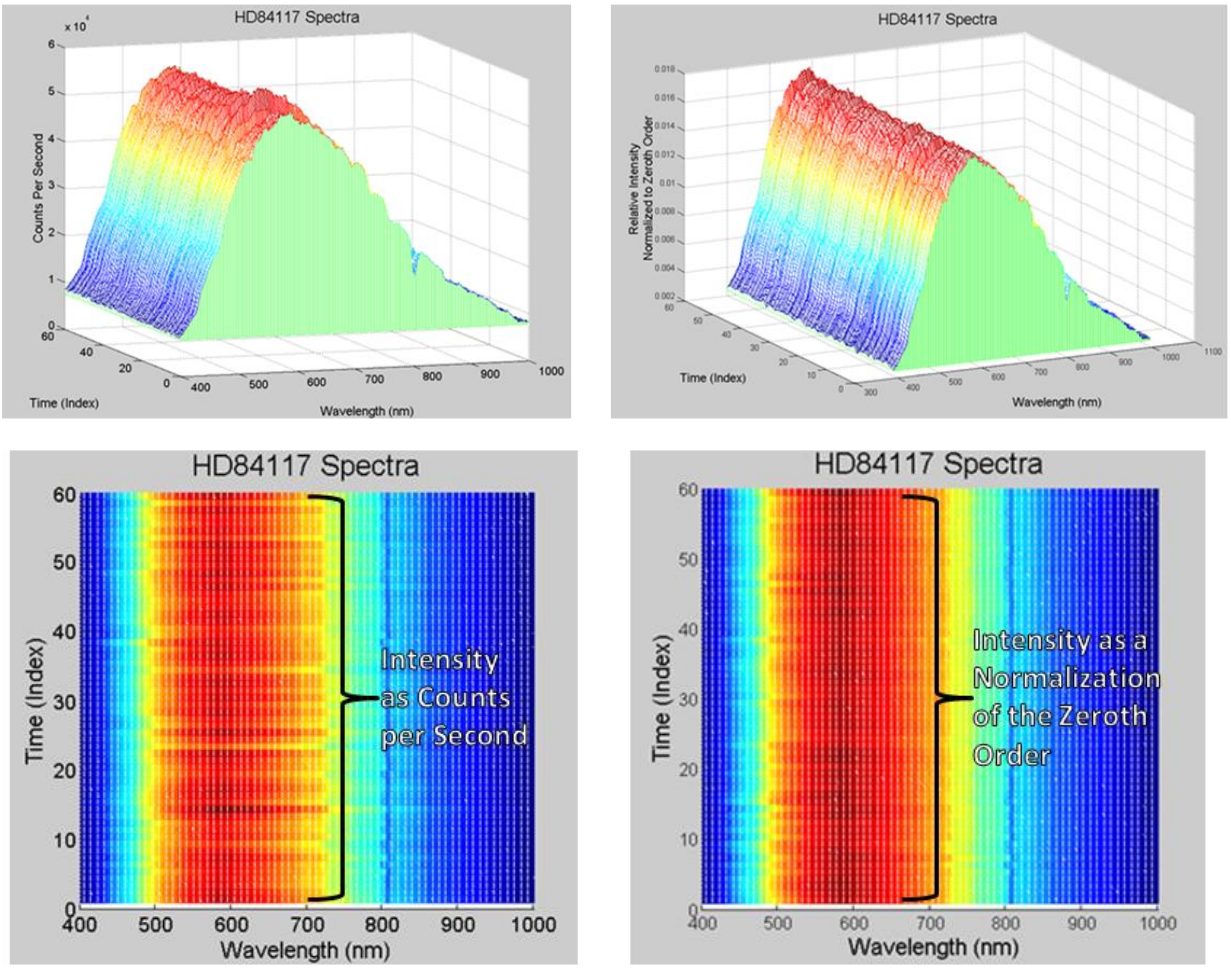

Fig. 10. Plot of the solar analog star HD 84117. The panels are the spectra in counts per second (top left panel) and relative intensity (top right panel). The bottom panels show the same spectra with a view from the z axis.

4. RESULTS

After removing the corrupt images from our series of satellite spectra, we processed the remaining images taken of the satellites, Wildblue-1 and DirecTV-12 (DTV-12). During early March 2015, we were fortunate enough to captured full glints for both of these satellites as we observed in real time from the raw camera images. The capture of the glint was further confirmed in the processed spectra as seen in Fig. 11 below. The figure shows a dramatic increase in the total counts per second in each frame from the beginning of the night to the end of the collection period (around 1,600 seconds after the start). Fig. 11 clearly depicts the intensity of Wildblue-1 increasing as it goes through a glint, but there are other more subtle spectral features corresponding to the glint that can be determined from the data.

For instance, Fig. 12 shows the average of 150 Wildblue-1 spectra taken before, during, and after the glint. The spectra before a glint (left panel) shows the peak of curve to be >550 nanometers as indicated by the leftmost arrow in the plot. During the glint (middle panel), we noticed that the peak shifted toward the blue end of the visible spectra to about 500 nanometers, and after the glint (right panel) the peak of the average spectra returned back to >550 nanometers. This appears to support our intuition that the main glint of a stable GEO satellite is caused primarily by its solar panels. Solar panels are designed to absorb solar flux, so it would make sense that since the majority of the solar energy is toward the red to near infrared end of the solar spectrum, a measured increase in a satellite's reflectance (i.e. a glint) would be toward the blue end. As a reference point to ensure there is no systematic bias in our spectra, the Fraunhofer O_2 absorption line (~760 nanometers) is used to maintain consistency

between the averages and is indicated by the rightmost arrow in each spectra. For all three averages this trough is around 775 nanometers, well within the resolution of our diffraction grating measurements.

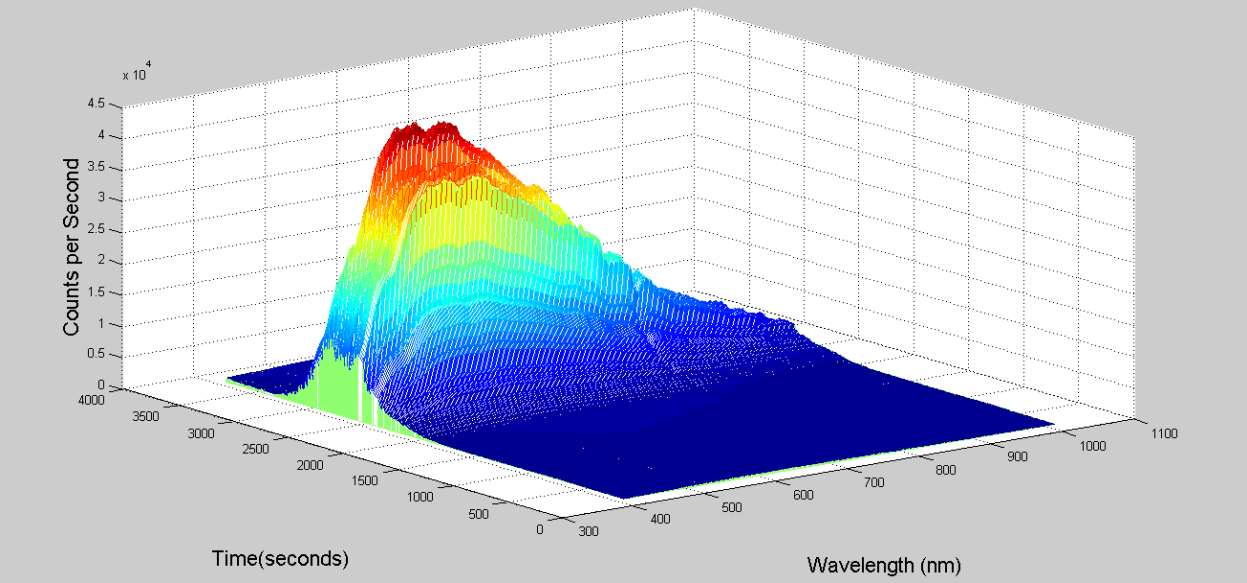

Fig. 11. Processed spectra for Wildblue-1 showing the increase in the count per second as a function of wavelength and time.

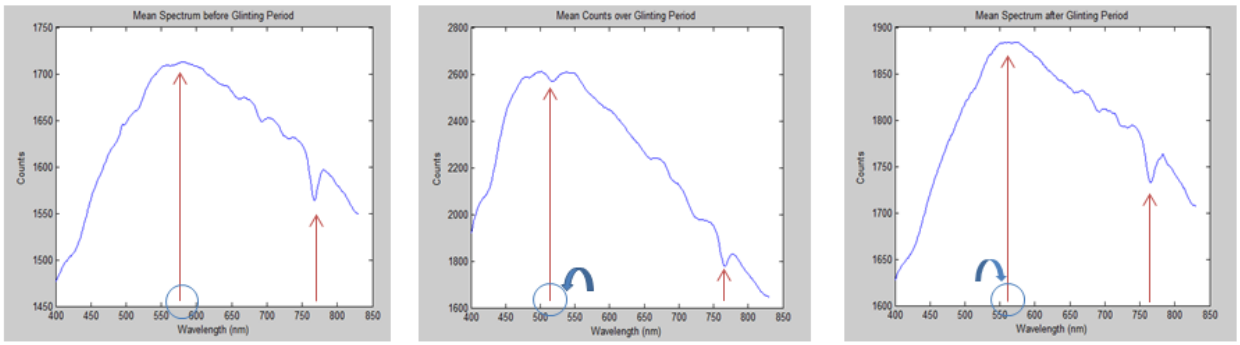

Fig. 12. Average spectra for Wildblue-1 before a glint (left panel), during a glint (middle panel), and after a glint (right panel).

Fig. 13 below shows the counts per second and normalized intensity plots of Wildblue-1 spectra. These plots are similar to the format of the plots seen in Fig. 10. The color shows relative intensity with blue being on the lower end and red being higher values. In the left plot, which is in counts per second, the glint can be very easily identified as the sudden increase in intensity between a time period from 2,500 to 3,000 seconds after the start of data collection. The black trace superimposed over the mesh shows the wavelength in each spectrum where the max counts per second occurs. Consistent with what we saw in Fig. 12, the peak of the spectra shifts from >550 nm to ~500 nm and back, before, during and after the glint. The O_2 absorption line is also easily seen around 775 nm. The right plot shows the spectra normalized to the zero order intensity; again the black trace indicates the wavelength in each normalized spectra where the maximum normalized intensity occurs. It is interesting to note that both plots show similar characteristic max intensity wavelength profile (i.e black traces) consistent with the solar panel as the source of the glint. Another interesting characteristic of the normalized mesh is that where the counts-per-second intensity mesh is high the normalized mesh is usually low. We speculate that this is due to the glint being more of a specular reflection whereas before and after the glint, the satellite's reflectance is more diffuse in nature. In fact, the normalized spectra of Wildblue-1 before the glint is very similar in appearance to the normalized spectra of the Wolf-Rayet HD84117 star which one would expect if the diffuse reflection properties are akin to a "blackbody" solar spectrum.

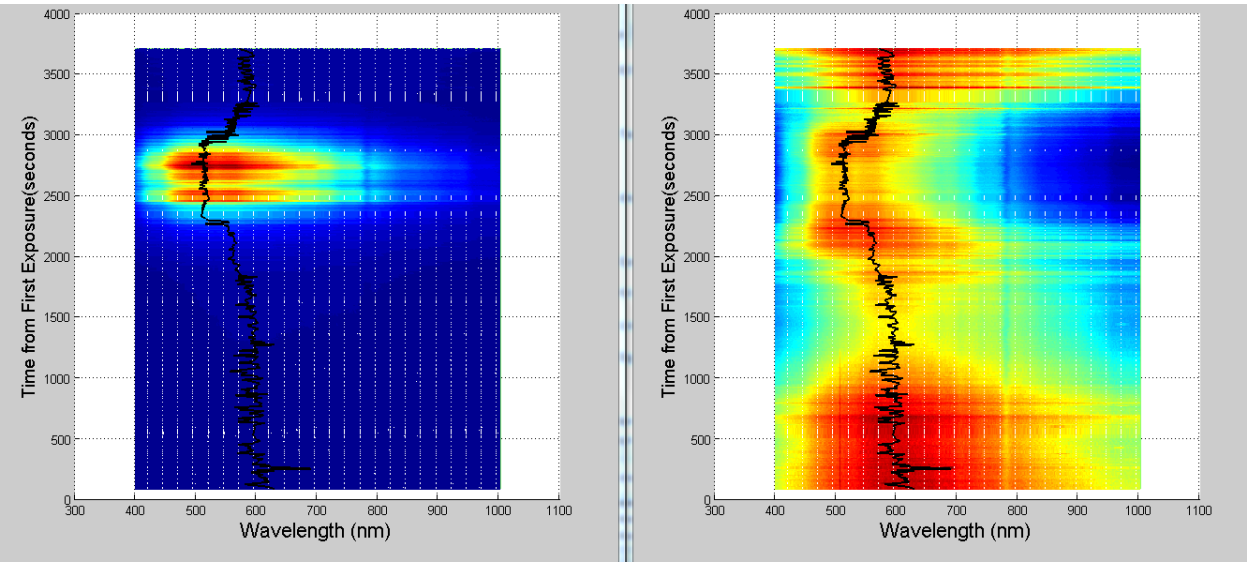

Fig. 13. Individual satellite spectra for Wildblue-1. The x axis for both is wavelength, while the y axis for both is time in seconds from the start of the data collection. The z axis for the left plot is in counts per second and normalized intensity (spectra normalized by the zero order) on the right plot.

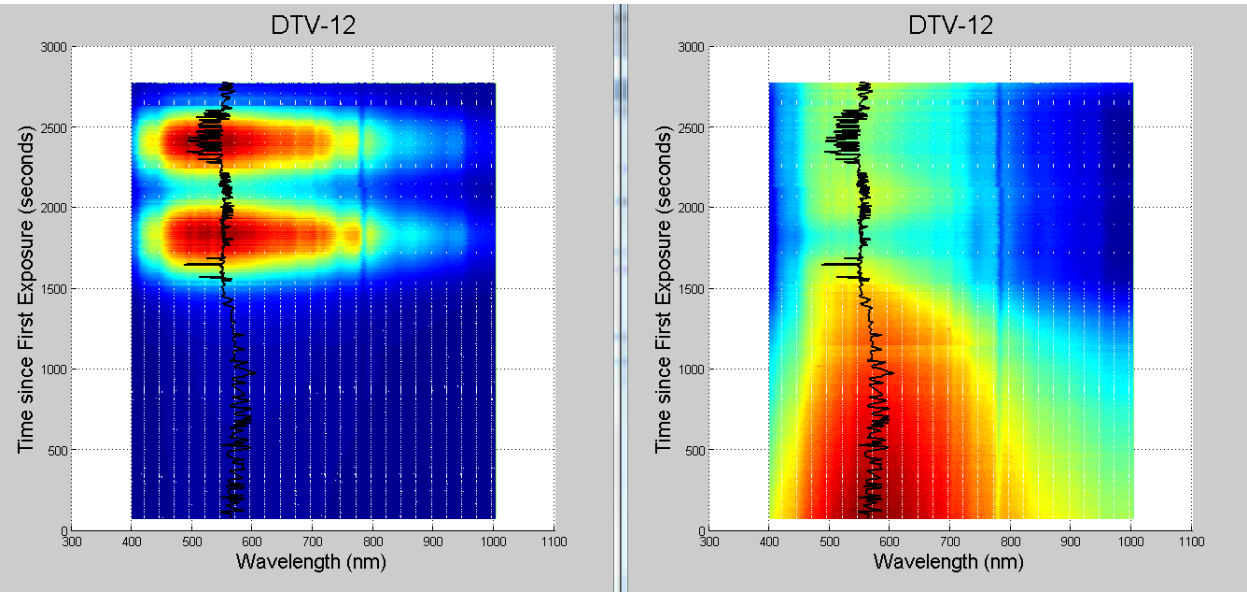

Fig. 14. Individual spectra for DTV-12 (same format as Fig. 10 and Fig. 13). The left plots are counts per second while the right plots are normalized intensity. The top plots are angled views, while the bottom plots are views from the z axis.

Fig. 14 is the meshplot of several DTV-12 spectra. The left plots are in counts per second versus time and wavelength and the right plots are the normalized intensities. As in Fig. 13, the black trace represents the wavelength for each spectra at which the counts per second (bottom left plot) or normalized intensity (bottom right plot) are maximum. There are noticeable differences between DTV-12 and Wildblue-1. Although DTV-12 has the same Boeing 702 spacecraft bus as Wildblue-1 and presumably very similar solar panels, DTV-12 shows a clear double glint (left plots) as opposed to a single glint for Wildblue-1. This double glint could be the result of the north and south solar panels on DTV-12 being offset in different east-west angles causing two glints, whereas the two solar panels of Wildblue-1 are both in the same east-west orientation. Additionally, the wavelengths where the maximum counts per second and normalized intensities (i.e., the black trace) occur do not move markedly toward the blue end of the spectrum during a glint as seen for Wildblue-1. The second glint appears slightly narrower in

time and exhibits much greater variability as depicted by the black trace. This could be an indication of solar panel difference or larger mechanical spacecraft structures causing glints in addition to the solar panels. Much like Wildblue-1 however, DTV-12's normalized intensity (bottom right plot) is out of phase with the counts per second spectra (bottom left plot), showing a more solar-like spectrum in non-glint conditions.

5. CONCLUSION

After analyzing the data we collected we were able to show that slitless spectroscopy can reveal many fine spectral features that broadband photometry simply cannot show. The full spectrum we collected on Wildblue-1 and DTV-12 showed a very clear shift in peak intensity from >550 nm to ~500 nm during glints. In addition to the shifting peak we found that the normalized glint profiles are in phase with the counts per second glint profiles. These results appear to support the contention that the primary source of a stabilized GEO satellite's glints is the solar panels. Future work will investigate the small-scale spatial and temporal features of a satellite's glint by removing as much of the solar spectrum as possible using a solar analog star. Additionally, more glint spectra measurements are warranted, especially to develop a baseline for a given GEO satellite.

6. ACKNOWLEDGEMENTS

The authors would like to thank the Air Force Office of Scientific Research whose funding supported this research.

7. REFERENCES

1. Payne, T.E., S.A. Gregory, N.M. Houtkooper, and T.W. Burdullis, "Classification of Geosynchronous Satellites Using Photometric Techniques", *Proceedings of the 2002 AMOS Technical Conference*, The Maui Economic Development Board, Inc., Kihei, Maui, HI, 2002.
2. Jorgensen, K., J. Okada, J. Africano, D. Hall, M. Guyote, K. Hamada, G. Stansbery, E. Barker, and P. Kervin, "Reflectance Spectra of Human-Made Space Objects," *The 2004 AMOS Technical Conference Proceedings*, The Maui Economic Development Board, Inc., Kihei, Maui, HI, 2004.
3. Hall, D., B. Calef, K. Knox, M. Bolden, and P. Kervin, "Separating Attitude and Shape Effects for Non-resolved Objects," *The 2007 AMOS Technical Conference Proceedings*, The Maui Economic Development Board, Inc., Kihei, Maui, HI, 2007.
4. Schildknecht, T., A. Vananti, H. Krag, andn C. Erd, "Reflectance spectra of space debris in GEO," *The 2009 AMOS Technical Conference Proceedings*, The Maui Economic Development Board, Inc., Kihei, Maui, HI, 2009.
5. Bédard, D., G. Wade, D. Monin, and R. Scott, "Spectrometric characterization of geostationary satellites," *Proceedings of the 2012 AMOS Technical Conference*, The Maui Economic Development Board, Inc., Kihei, Maui, HI, 2012
6. Hoag A. and D. Schroeder, "Nonobjective grating spectroscopy", *Publications of the Astronomical Society of the Pacific*, Vol. 82, No. 489 (October 1970), pp. 1141-1145.
7. Payne, T. E., S.A. Gregory, S. A., and K. Luu, "SSA Analysis of GEOS Photometric Signature Classifications and Solar Panel Offsets," *Proceedings of the 2006 AMOS Technical Conference*, The Maui Economic Development Board, Inc., Kihei, Maui, HI, 2006.
8. Tippets, R.D., S. Wakefield, S. Young, I. Ferguson, C. Earp-Pitkins, and F.K. Chun, "Slitless Spectroscopy of Geosynchronous Satellites," *accepted by Optical Engineering*, 2015.
9. Vrba, F.J., M.E. DiVittorio, R.B. Hindsley, H.R. Schmitt, J.T. Armstrong, P.D. Shankland, D.J. Hutter, and J.A. Benson, "A survey of geosynchronous satellite glints." *The 2009 AMOS Technical Conference Proceedings*, The Maui Economic Development Board, Inc., Kihei, Maui, HI, 2009.
10. West, D., "Resolution Calculation for a Slitless Spectrograph," URL: http://users.erols.com/njastro/faas/articles/west01.htm [cited 2 September 2015].
11. Wikipedia contributors. "Solar analog." *Wikipedia, The Free Encyclopedia*. Wikipedia, The Free Encyclopedia, 7 Apr. 2015. Web. 2 Sep. 2015.